

**Dielectric function of a poly(benzimidazobenzophenanthroline) ladder polymer**S. Kraner,<sup>\*</sup> C. Koerner, and K. Leo*Institut für Angewandte Photophysik, Technische Universität Dresden, 01062 Dresden, Germany*

E. Bittrich, K.-J. Eichhorn, Y. Karpov, A. Kiriy, and M. Stamm

*Leibniz-Institut für Polymerforschung Dresden, 01069 Dresden, Germany*

K. Hinrichs

*Leibniz-Institut für Analytische Wissenschaften - ISAS - e.V., Department Berlin, 12489 Berlin, Germany*

M. Al-Husseini

*Department of Physics, The University of Jordan, Amman 11942, Jordan*

(Received 1 December 2014; revised manuscript received 3 March 2015; published 11 May 2015)

The dielectric function and the effective conjugation length of an organic material determine the binding energy of an exciton formed after photon absorption. In ladder polymers the conjugation length is large and the size of the exciton is in principle not limited by its conjugation length, since it can delocalize along the backbone of the polymer. In this work, the anisotropic dielectric function of poly(benzimidazobenzophenanthroline) (BBL) in the UV-visible and infrared spectral range is obtained by DFT calculations and by modeling ellipsometric data, revealing both ionic and electronic contributions. For spin-coated BBL polymer thin films, we show uniaxial anisotropic behavior with high differences between the in-plane and out-of-plane dielectric function. We obtain a high dielectric constant of 8.3 in the direction of the polymer.

DOI: [10.1103/PhysRevB.91.195202](https://doi.org/10.1103/PhysRevB.91.195202)

PACS number(s): 77.55.dj, 88.40.fc, 88.40.jr, 82.20.Wt

**I. INTRODUCTION**

Organic photovoltaics provide a promising technology in order to complement inorganic solar cells. Although much research effort has doubled the power conversion efficiency (PCE) of organic solar cells in the last five years up to 12%, the PCE is still low compared to the inorganic devices. The physical steps in a solar cell can be simplified to absorption of a photon, exciton dissociation, and charge transport to electrodes. Thus, a material for a solar cell should have a high absorption coefficient, an efficient exciton separation process, and holes and electrons should be transported to the electrodes with minimized recombination. The power of organic materials consists not only in the low cost, but especially in the tunability of physical properties. In order to increase the efficiency, new absorber dyes are synthesized to absorb more sunlight in a tandem or cascade configuration [1–3]. The main loss mechanism of organic solar cells, however, is expressed in the low open-circuit voltage. This is related to the usually tightly bound exciton in these materials, leading to an energy loss for separation. It is thus of great importance to reduce the exciton binding energy ( $E_B$ ).  $E_B$  is the fundamental difference between organic and inorganic solar cells. For a Wannier-Mott exciton, the exciton binding  $E_{BW}$  energy can be described by a modified hydrogen model, whereas the binding energy of a Frenkel exciton  $E_{BF}$  is defined by the Coulomb attraction of a hole and an electron:

$$E_{BW} = \frac{a_0 E_R}{a_{EW} \epsilon_r}, \quad a_{EW} = a_0 \frac{m_e \epsilon_r}{\mu}, \quad E_{BF} \approx \frac{e^2}{4\pi \epsilon_0 \epsilon_r a_{EF}}, \quad (1)$$

with the dielectric constant  $\epsilon_r$ , the reduced mass  $\mu$ , the rest mass of electron  $m_e$ , the Bohr radius  $a_0$ , the elementary charge  $e$ , the Rydberg energy  $E_R$ , and the exciton radius for the Wannier and Frenkel exciton are  $a_{EW}$  and  $a_{EF}$ , respectively. These equations suggest that  $E_{BW}$  or  $E_{BF}$  can be lowered by increasing  $\epsilon_r$ . For the Wannier exciton this results in a larger  $a_E$ . Leblebici *et al.* show an increased open-circuit voltage and an increased internal quantum efficiency by blending a high dielectric small molecule into the donor [4]. A lower geminate recombination rate was achieved by adding polar side chains to the donor polymer of a bulk heterojunction solar cell, leading to a higher dielectric constant [5]. Camaioni *et al.* show the potential of high dielectric organic materials and make suggestions for materials such as the dendrimers reported by Guo [6,7].

Materials with an exciton binding energy smaller than  $k_B T$  ( $\approx 25$  meV at room temperature) generate free charge carriers upon absorbing a photon, since the thermal excitations of the material can break the bound excitonic state. Gallium nitride (GaN) has an exciton binding energy of 20 meV [8], and is therefore close to the threshold to form free charges at room temperature. Its exciton radius is 3.9 nm and the dielectric constant is 9.8 [8,9]. Excitons in most small organic molecules are localized and scale with the size of the molecule [10]. Therefore, larger conjugated systems could possess lower exciton binding energies, which has been already confirmed theoretically [11,12]. Indeed, a correlation of the exciton binding energy with the molecule length was measured [13]. The low binding energy in poly(2-decyloxy-1,4-phenylene) (DO-PPP) was explained as a consequence of the size of the molecule, which was determined to be 9 nm. Therefore, it is important that the  $\pi$  system on the absorber molecule is not interrupted. From the above analysis we conclude that organic materials might generate free charges after absorbing

<sup>\*</sup>stefan.kraner@iapp.de

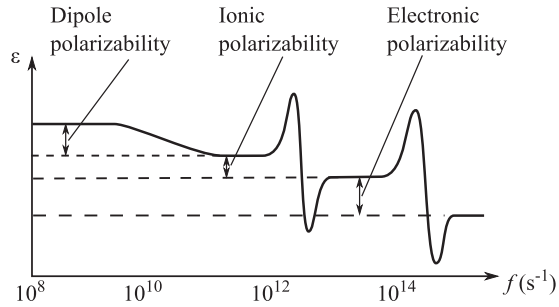


FIG. 1. Sketch of a dielectric function with dipole, ionic, and electronic contributions shown at their specific frequencies [17].

a photon if the dielectric constant is higher than about 10 and the  $\pi$  system expands uninterrupted over more than about 8 nm ( $\approx 2a_E$ ).

Several high-dielectric organic materials have been reported, among them the previously mentioned dendrimers from Guo with a dielectric constant of 15 [7], and the oriented PPV from Moses with a dielectric constant of 8–10 and an exciton binding energy of 60 meV [14]. Yoon *et al.* showed that highly oriented self-assembled monolayers can reach a high dielectric constant. Stilbazolium layers (Stb) deliver a high polarizability. This leads to a dielectric constant of 16 perpendicular to the substrate [15]. Polymers such as homochiral 1D zinc-quitenine coordination polymers have a dipole moment which induce a high dielectric constant of 37.3 [16]. The dielectric constant (or dielectric function) depends strongly on the frequency. In Fig. 1 the different contributions are depicted. Since many of the cited high dielectric organic materials were measured by impedance spectroscopy at frequencies up to 1 MHz, it is questionable whether their behavior can be extrapolated to the appropriate frequency regime of 1–100 THz ( $\approx E_B/h$ ). For example, dipole polarizabilities can strongly contribute to the dielectric constant, but their reaction time is too slow and an exciton would recombine before the dipoles begin to move.

Organic materials can have high mobilities [18,19], high dielectric constants, and can have different colors as can be seen in nature. Therefore, in principle the needed physical properties are provided. Thus, the question arises, how can the different properties in organic materials be combined to get an efficient solar cell? By reducing  $E_B$  below 25 meV, the same PCEs as in the inorganic solar cells could be achieved with the advantage of lower production costs.

In this work, we focus on a ladder-type polymer poly(benzimidazobenzophenanthroline) (BBL) in order to provide a system with a conjugation length larger than 8 nm. The dielectric function is measured by ellipsometric techniques and is compared to DFT calculations, leading to a dielectric constant of about 8.3 along the backbone of the polymer. The dielectric constant perpendicular to the polymer is around 3. We show how the ionic contribution to the dielectric constant can be calculated with *ab initio* simulation techniques. Comparing ionic and electronic contributions to the dielectric constant, we show that the ionic part has a minor but not negligible influence.

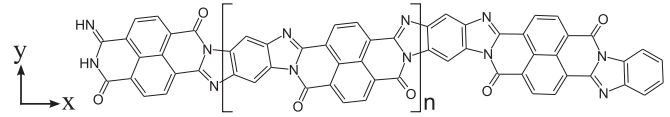


FIG. 2. Chemical structure of 3 monomers with a statistically distributed oxygen orientation in the polymer chain.

## II. MEASUREMENTS

The structure of the planar polymer is shown in Fig. 2, where due to synthesis reasons, a statistical distribution of oxygen atoms on both sides of the polymer chain is present [20]. It is known that the BBL polymer packs in an orthorhombic structure. When films are spin coated on glass, the unit cell stands perpendicular to the substrate, whereas the backbone is parallel to the substrate [21,22], which is shown in Fig. 2. In order to obtain the dielectric function, we performed ellipsometry measurements in the infrared (IR) and UV-visible spectral range. For the IR ellipsometry, BBL was spin coated on a silicon substrate with native  $\text{SiO}_2$ , whereas for the UV-visible ellipsometry a silicon substrate with 1  $\mu\text{m}$   $\text{SiO}_2$  was used. Grazing-incidence wide-angle x-ray scattering (GIWAXS) data, shown in Fig. 3, reveal a reflection along the meridian, which indicates a highly oriented structure of the polymer film. The broad outer ring is mainly due to the 1  $\mu\text{m}$   $\text{SiO}_2$  layer (see Fig. 7). Shown in Fig. 4 are an out-of-plane line cut of Fig. 3 and an XRD curve of a BBL powder sample. In both curves two peaks are visible. They belong to the  $\pi$  stacking in the  $z$  direction (010) with a distance of  $d_z = 3.78 \text{ \AA}$  and to the stacking in the  $y$  direction (100) with a distance of  $d_y = 8.39 \text{ \AA}$ . Both lattice constants are therefore slightly higher than previously reported [21], which might originate from slightly different conditions during synthesis of the polymer and preparation of the thin film. The peak at 3.78  $\text{\AA}$  is attributed to the (010) direction. Since the monomer polymerizes in different orders (Fig. 2), which leads a statistical distribution of oxygen atoms on both sides of the polymer backbone, no peak in the  $x$  direction (001) is visible.

It was shown that interference-enhanced ellipsometry can be used to quantify anisotropic behavior of conjugated organic thin films [23–25]. Figure 5 shows the imaginary and real

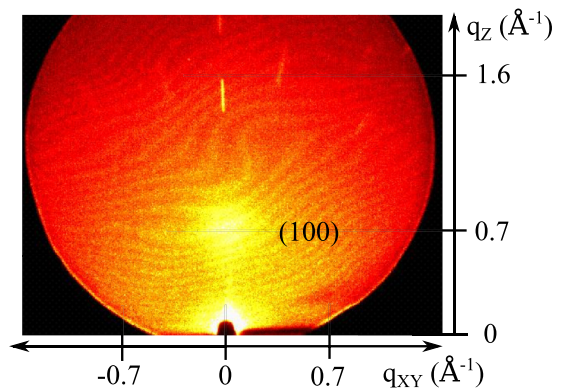


FIG. 3. (Color online) GIWAXS data from BBL on a silicon substrate.

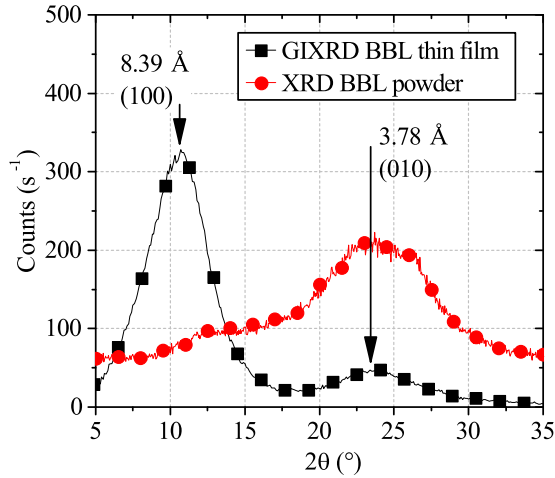


FIG. 4. (Color online) XRD patterns from BBL powder and from a BBL thin film.

part of the dielectric function in the IR and UV-visible regime. The birefringence at 1680 nm and therefore with electronic contributions only is  $\Delta n = n_{\text{in plane}} - n_{\text{out of plane}} = 2.08 - 1.7 = 0.38$ . Compared to other spin-coated systems, the refractive anisotropy is high [23], which supports the conclusions from the GIWAXS data, i.e., the highly oriented structure of BBL in spin-coated devices. According to Eq. (2) discussed below, the dielectric function is connected with the polarizability. The anisotropy in the UV-visible regime is due to a high electronic polarizability in-plane compared to out-of-plane. In-plane the extended  $\pi$  system from the ladder polymer backbone and the  $\pi$  stacking is present.

It is known that highly oriented conjugated polymers can have a high dielectric constant in the direction of the backbone [14]. The higher dielectric function in-plane originates from the uninterrupted  $\pi$  system along the polymer, which lies parallel to the substrate.

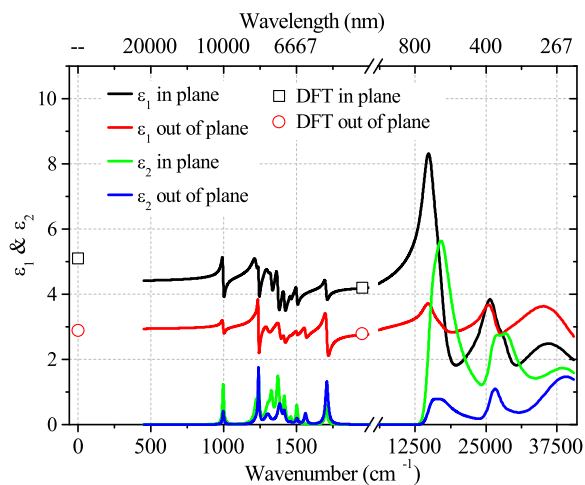


FIG. 5. (Color online) Real ( $\epsilon_1$ ) and imaginary ( $\epsilon_2$ ) part of the dielectric function of a spin-coated BBL film, measured by IR and UV-visible ellipsometry. The dots are calculated by DFT with and without ionic contributions.

Oxygen and nitrogen form partially covalent and partially polar bonds to carbon. The polar part of the molecule contributes to the ionic part of the dielectric function which corresponds to the difference between  $\epsilon_1$  at  $2000 \text{ cm}^{-1}$  and at  $500 \text{ cm}^{-1}$ , which is in-plane  $\Delta\epsilon_1 = 0.23$  and out-of-plane  $\Delta\epsilon_1 = 0.17$ . At  $1707 \text{ cm}^{-1}$  we can see the vibronic stretching contribution of a C=O double bond. The imaginary part  $\epsilon_2$  out-of-plane at  $1707 \text{ cm}^{-1}$  is higher than in-plane, which shows the preferential orientation of the C=O bonds perpendicular to the substrate. Since the C=O has a certain angle to the polymer backbone (see Fig. 2), a smaller contribution of  $\epsilon_2$  is still visible in-plane.

### III. CALCULATIONS

In this section the dielectric function is modeled in order to divide the in-plane contribution into a part along the backbone and the direction of the  $\pi$  stacking. Intermolecular interactions are neglected.

The Clausius-Mossotti equation delivers the relation between the molecular polarizability volume  $\alpha'$  and the dielectric function  $\epsilon_r$  in the bulk. It is valid for nonpolar materials and for cubic or amorphous structures:

$$\frac{\epsilon_r - 1}{\epsilon_r + 2} = \frac{4\pi}{3} \frac{1}{V_M} \alpha', \quad (2)$$

where  $V_M$  is the molecular volume. For anisotropic media  $\epsilon_r$  and  $\alpha'$  are tensors. If these tensors are diagonal, one can simply solve Eq. (2) for each axis ( $x, y, z$ ) [26–28]. Isolating  $\epsilon_r$  gives the relation used for the  $y$  and  $z$  direction of the polymer. To consider the noncubic orthorhombic structure, we normalize the polarizability volume  $\alpha'$  in the  $y$  and  $z$  directions with a factor  $V_M^{1/3}/d_y$  and  $V_M^{1/3}/d_z$  for the  $y$  and  $z$  directions, respectively. Srinivasan *et al.* show that in order to prevent the *Mossotti catastrophe* for anisotropic crystals the Clausius-Mossotti equation is extended with a depolarization factor determined by Osborn [29,30]. The depolarization factor for a sphere is  $\frac{4\pi}{3}$ , resulting in the Clausius-Mossotti equation (2). For a polymer one can approximate the shape in the direction of the backbone ( $x$ ) with an infinite cylinder with a depolarization factor of 0, leading to [29,30]

$$\epsilon_{rx} = 1 + 4\pi \frac{\alpha'_x}{V_M}. \quad (3)$$

To calculate the in-plane and the mean dielectric constant, the polarizabilities in each direction can be added up ( $\alpha'_{\text{mean}} = (\alpha'_x + \alpha'_y + \alpha'_z)/3$ ,  $\alpha'_{\text{in plane}} = (\alpha'_x + \alpha'_z)/2$  [31,32]) as long as the Clausius-Mossotti equation is valid, which is not the case in the  $x$  direction, since the depolarization factor is needed. To get  $\alpha'_x$  (for a cubic structure) from  $\epsilon_{rx}$  we use Eq. (2). With this approach we calculate the dielectric function with respect to the axis in the molecular plane. The subsequent calculations were made with the basis set def2-SVPD and the hybrid functional PBE0 on the software platform TURBOMOLE [33–43] (for more information see Appendix B).

#### A. Electronic polarizability

In Fig. 6, the electronic polarizability volume per monomer unit is shown for different calculated numbers of monomers.

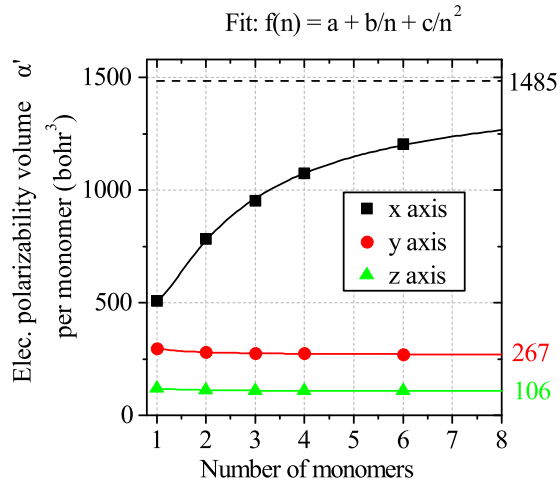


FIG. 6. (Color online) Calculated electronic polarizability volume per monomer unit of 1 to 6 monomers of BBL. The dots represent calculated points. The lines are fitting curves according to the shown polynomial function, and  $n$  is the number of monomers. The numbers at each curve indicate the limit for  $n \rightarrow \infty$ , i.e., long polymers.

A longer polymer backbone clearly indicates a higher polarizability in the  $x$  direction. Ruuska *et al.* reported a similar behavior for polypropylene [28]. For an infinite polymer a saturation is expected, which can be fitted by the equation  $a + b/n + c/n^2$ , where  $a$ ,  $b$ , and  $c$  are parameters, and  $n$  is the number of monomers [44]. A fit with a saturation of the electronic polarizability volume along the backbone of 1485 bohr<sup>3</sup> is shown in Fig. 6. The relative polarizabilities in the  $y$  and  $z$  direction do not increase with higher numbers of monomers, since in those directions the polarizability scales with the molecular weight of the simulated molecule and thus the molecular polarizability per monomer unit should stay constant. Nevertheless, probably due to the relatively lower amount of hydrogen atoms for larger molecules, a saturation is observed as well.

### B. Ionic polarizability

In addition to the electronic polarizability calculated in the last section, we introduce here a new concept to calculate the ionic part of the polarizability by DFT. Applying an electric field on a solid with ionic or partially ionic bonds results not only in the movement of electrons but also in the movement of the (partially) charged nuclei, which are lower in frequency but contribute to the static dielectric constant as well. The geometry optimization in DFT (TURBOMOLE) delivers the dipole moment of the molecule. Calculating the difference of the dipoles from geometry optimizations with and without an applied electric field gives the induced dipole moment. Dividing the induced dipole moment by the applied electric field results in the polarizability, which should stay constant at different electric fields. For low electric fields [ $<1 \times 10^{-4}$  atomic units (a.u.)] the numerical error becomes large, whereas for high electric fields ( $>0.01$  a.u.) the distortion of the molecule is high and therefore it also changes the electronic part of the polarizability. Since the polarizability is defined for small electric fields, they are chosen as low as

possible, i.e., between 0.002 and 0.0002 a.u., which is in the range of an electric field generated by a pair of opposite charges with a distance of 3 to 10 nm. Thus, the values are in the same order of magnitude as the electric field between an electron and a hole forming an exciton. Using the electric fields mentioned above to calculate the polarizability volume  $\alpha'$  of H<sub>2</sub>O in gas phase, a value of  $\alpha' = 1.49 \times 10^{-24}$  cm<sup>3</sup> is obtained, which is similar to the reported value of  $\alpha' = 1.45 \times 10^{-24}$  cm<sup>3</sup> [45].

Table I shows the electronic polarizability volume  $\alpha'$  obtained from DFT calculations (see Fig. 6) and the combination of electronic and ionic polarization calculated by electric fields applied. The difference between both is attributed to the ionic contribution of the polarizability. For the polarizability calculations an electric field in the  $x$ ,  $y$ , and  $z$  directions has to be applied to get the polarizability tensor. As a self-test for the accuracy of DFT, the tensor must be symmetric, which is the case for the reported polarizabilities.

### C. Dielectric constant

To obtain the dielectric constant, Eqs. (2) and (3) for the  $y$ ,  $z$  directions and for the  $x$  direction are used, respectively. A lattice parameter in the  $x$  direction of 12.16 Å is defined as a mean value from DFT, whereas in the  $y$  and  $z$  directions the lattice parameters are taken from GIXRD measurements, corresponding to 8.39 Å and 3.78 Å, respectively. This procedure results in a molecular volume of  $V_M = 2602$  bohr<sup>3</sup> = 386 Å<sup>3</sup>.

The calculated dielectric constants are shown in Table I and in Fig. 5. The influence of the ionic contribution to the dielectric constant in the  $x$  and  $y$  directions is below 6%. For the  $z$  component, the ionic contribution to the dielectric constant is about 27%. The ionic contribution to the polarizability volume for all directions lies between 13 and 37 bohr<sup>3</sup>, which is small compared to the electronic polarizability volume in the  $x$  direction of 1485 bohr<sup>3</sup>.

The numerical error from the DFT calculations is about 2.4%. The chosen fit for the polarizability has a larger impact on the asymptotic value for an infinite polymer length, shown in Fig. 6. Fitting by an exponential curve, proposed by Champagne *et al.* [46], gives an electronic polarizability of 1302 bohr<sup>3</sup>. This would change the static dielectric constant to 7.5 in the  $x$  direction.

## IV. DISCUSSION

The transition energies obtained from UV-visible ellipsometry measurements in-plane and out-of-plane of spin-coated BBL are in good agreement with the DFT calculations, as shown in the electronic dielectric function in Fig. 5. For the out-of-plane direction the ionic contributions to the dielectric constant fit to the DFT calculations as well, but in-plane, the calculations seem to overestimate the ionic contribution. This deviation comes from the experimentally inaccessible frequency range below 400 cm<sup>-1</sup>. It is confirmed by a vibrational analysis of TURBOMOLE that the rocking mode of double-bonded oxygen is below 400 cm<sup>-1</sup>, and is therefore not accessible by the used infrared ellipsometry setup. To estimate the impact of this mode on the ionic contribution, we freeze all other atoms and the C=O bond length during the geometry

TABLE I. Anisotropic polarizability volume ( $\text{bohr}^3$ ) of a BBL monomer and the corresponding dielectric constant.  $x$ ,  $y$ , and  $z$  directions refer to Figs. 6 and 2.

	Polarizability volume			Dielectric constant					
	$x$	$y$	$z$	$x$	$y$	$z$	in-plane	out-of-plane	mean
Elec	1485	267	106	8.2	2.8	2.5	4.2	2.8	3.6
Ionic	34	13	37						
Elec.+ionic	1519	280	143	8.3	2.9	3.4	5.1	2.9	4.2

optimization with an applied electric field; see Sec. III B. It turns out that the rocking mode contributes to the polarizability volume with a value of  $15 \text{ bohr}^3$  in the  $x$  direction. Subtracting this value from the polarizability in the  $x$  and  $z$  directions, we get a dielectric constant of 4.7 for the in-plane component, which is already close to the measured 4.4 at  $500 \text{ cm}^{-1}$ . This explains in part the observed gap between the measured low frequency and the calculated static dielectric constant.

## V. CONCLUSIONS

The dielectric function of spin-coated BBL films in the UV-visible and IR regime exhibits a highly anisotropic behavior. This finding is attributed to the known ordering of BBL on a glass substrate, i.e., the backbone is parallel, and the molecular plane perpendicular to the glass substrate. The contributions of the ionic and electronic parts to the dielectric function have been identified. The measured dielectric function matches well with the DFT calculations, which reveal a dielectric constant of 8.3 in the direction of the polymer and around 3 perpendicular to the backbone (see Table I).

Increasing the electronic dielectric function might be possible by a broader  $\pi$  system in order to increase the number of  $\pi$  electrons contributing to the screening effect. Increasing the ionic part of the dielectric function might also be successful in order to decrease the exciton binding energy, since their vibrational frequencies can still be higher than  $\approx E_B/h$  and would therefore contribute to the screening of an exciton as well. This could be achieved with an increasing number of partially polar bonded atoms in the ladder polymer.

## ACKNOWLEDGMENTS

The authors would like to thank Dr. Lutz Wilde for performing GIXRD measurements at the Fraunhofer CNT in Dresden. We are also thankful to Koen Vandewal and Reinhard Scholz for reviewing and helpful discussions. K.H. thanks Ilona Engler for technical assistance. Financial support by the Senatsverwaltung für Wirtschaft, Technologie, und Forschung des Landes Berlin und Bundesministerium für Bildung und Forschung is gratefully acknowledged. M.A.H. thanks The University of Jordan and Leibniz-Institut für Polymerforschung Dresden e. V. for financial support.

## APPENDIX A: EXPERIMENTAL DETAILS

### 1. Synthesis of BBL

Starting materials for the synthesis were purchased from Sigma-Aldrich (polyphosphoric acid, methanesulfonic

acid), TCI (1,4,5,8-naphthalenetetracarboxylic acid), and Leap Chem (1,2,4,5-tetraaminobenzene tetrahydrochloride), and used as received. Synthesis was done according to a modified procedure [20]. To a 500 ml three-necked flask with a magnetic stirrer and argon inlet and outlet 300 g of polyphosphoric acid was added. It was vacuumed and deoxygenated by heating at  $100 \text{ }^\circ\text{C}$  for 4 hours. Under argon atmosphere at  $110 \text{ }^\circ\text{C}$  5.68 g (20 mmol) of 1,2,4,5-tetraaminobenzene tetrahydrochloride was added and heated overnight until all the hydrogen chloride was thermally displaced from the tetramine. Then under argon atmosphere 6.08 g (20 mmol) of 1,4,5,8-naphthalenetetracarboxylic acid was added and the mixture was heated to  $180 \text{ }^\circ\text{C}$  and maintained at this temperature for 7 hours. The resulting dark-red solution was poured out of the flask and after cooling to room temperature dissolved in 3 l of methanol. The dark-brown precipitate was filtrated, washed with a large amount of methanol until the filtrate was colorless, and dried at  $200 \text{ }^\circ\text{C}$  under reduced pressure. Precipitation from 250 g of methanesulfonic acid and drying in the described manner gave 6.48 g (97%) of polymer.

### 2. Sample preparation

0.3 wt. % BBL was dissolved in methane sulfonic acid (MSA) at  $100 \text{ }^\circ\text{C}$ . The solution was then filtered with a  $1.2 \mu\text{m}$  pore size PTFE filter. To improve the adhesion of BBL to the glass, the substrates were cleaned in oxygen plasma and then dipped into (3-Mercaptopropyl) trimethoxysilane (MPTMS). The residual MPTMS was washed out by isopropanol. The substrates were spin coated at 800 rpm for 40 seconds. After spin coating the film still has MSA inside, which can be seen by a reddish color. After waiting two minutes, giving the molecules time to arrange themselves, the substrate was dipped into deionized water for one minute. The color of the film now turned from red to blue, since the MSA was washed out. Then the film was dried with compressed nitrogen. To wash the residual MSA out of the film, the substrate was again immersed in deionized water for 14 hours. After drying with nitrogen the film was heated at  $150 \text{ }^\circ\text{C}$  for 2 hours to remove the water.

### 3. Powder XRD

XRD curves were obtained for powder samples using a 2-circle diffractometer (XRD 3003 T-T, Seifert-FPM) and a point detector. By employing a parabolic multilayer mirror, a highly parallel beam of monochromatic  $\text{Cu-K}\alpha$  radiation ( $\lambda = 1.5418 \text{ \AA}$ ) was obtained.

#### 4. GIWAXS

Grazing-incidence wide-angle x-ray measurements (GIWAXS) were performed using a Bruker D8 Discover diffractometer operating at 1.6 kW. The diffractometer is equipped with a Cu Twist tube, Ni filter ( $\lambda = 1.5418 \text{ \AA}$ ), point focusing PolyCap system for parallel beam generation, and 0.3 mm PinHole collimator for the incident beam. The sample was mounted on an Eulerian cradle with automatic controlled XYZ stage. The GIWAXS patterns were recorded with a VNTEC-500 area detector using a sample-to-detector distance of 155 mm and an incident angle of  $0.5^\circ$ . To extract quantitative information, the intensity is integrated over arc slices taken from the 2D GIWAXS pattern using Bruker LEPTOS software.

#### 5. GIXRD

GIXRD measurements have been carried out on a Bruker D8 Discover diffractometer. A third-generation 60 mm Göbel mirror was used to parallelize Cu  $K\alpha$  radiation from an x-ray tube operated at 40 kV and 40 mA. The incidence angle was set to the critical angle for total external reflection ( $\omega = 0.2^\circ$ ). The diffracted intensity depending on the detector angle was collected in the range between  $3^\circ$ - $90^\circ$  with a step size of  $0.1^\circ$  and 30 s sampling time per step.

#### 6. UV-visible ellipsometry

UV-visible ellipsometry investigations were performed using a spectroscopic ellipsometer (M2000 UI, J. A. Woollam Co., Inc.) at five different angles of incident light ranging from  $55^\circ$  to  $75^\circ$  in steps of  $5^\circ$ . At each angle of incidence, the ellipsometric angles  $\Delta$  and  $\Psi$  were measured throughout the spectral region from 245 to 1680 nm. The values of  $\Delta$  and  $\Psi$  did not change when rotating the samples in the horizontal  $xy$  plane, showing that no in-plane anisotropy is present. Thus the samples are either isotropic or uniaxial anisotropic with the optical axis perpendicular to the substrate surface. The analysis of the measured data was performed using the CompleteEASE software from J. A. Woollam Co., Inc. A detailed discussion of ellipsometry can be found in the literature [47–49]. A uniaxial anisotropic optical model of five oscillators (two Tauc-Lorentz, three Gaussian) in-plane and out-of-plane was used to fit the experimental ellipsometric angles. Energetic positions of the oscillators in-plane and out-of-plane were coupled, in order to reduce the number of fit parameters. Roughness of the sample was modeled by using an effective medium approximation (EMA) top layer with 50% void and 50% of the polymer. The thickness of the roughness top layer was 5 to 7 nm. Uniaxial anisotropy of the samples was evaluated by the birefringence, i.e., different refractive index in ordinary (in-plane) and extraordinary (out-of-plane) direction to the optical axis, and by the order parameter  $S$  [24,25]. The latter can be calculated from the extinction coefficients  $k_{\text{in plane}}$  and  $k_{\text{out of plane}}$ , and is connected to the angle  $\theta$  between the molecular transition dipole and the direction perpendicular to the substrate surface given by

$$S = P_2(\cos \theta) = \frac{1}{2}(3 \cos^2 \theta - 1) \\ = \frac{k_{\text{out of plane}} - k_{\text{in plane}}}{k_{\text{out of plane}} + 2k_{\text{in plane}}}, \quad (\text{A1})$$

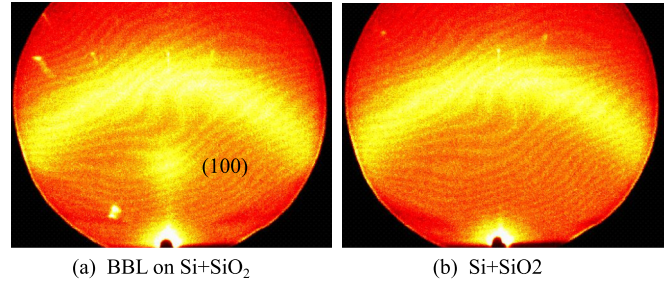


FIG. 7. (Color online) (a) GIWAXS data from BBL on a substrate with  $1 \mu\text{m SiO}_2$ . (b) GIWAXS data from a bare silicon substrate with  $1 \mu\text{m SiO}_2$ .

where  $P_2(\cos \theta)$  is the second Legendre polynomial and  $\langle \dots \rangle$  is the ensemble average. The ensemble average tilt angle of the molecular transition dipole is determined from the measured maximum extinction coefficients at a wavelength of 560 nm.

#### 7. IR ellipsometry

The IR ellipsometric measurements were performed with a custom-built photometric rotating polarizer ellipsometer [49–51], externally attached to a BRUKER 55 Fourier transform spectrometer. The probed spot on the surface was approximately  $40 \text{ mm}^2$  at  $65^\circ$  incidence angle. Measurements were taken at  $55^\circ$ ,  $60^\circ$ , and  $65^\circ$  with  $\text{cm}^{-1}$  spectral resolution with a DTGS (deuterated triglycine sulfate) detector. SpectraRay/3 software from SENTECH Instruments, Germany, served for the simulations of the infrared ellipsometric data in an optical layer model air/polymer/silicon. The vibrational bands of the polymer were described with Lorentz oscillators in an uniaxial polymer layer [52]. Fit parameters were the direction-dependent oscillator parameters such as resonance frequencies, strengths, and half widths.

#### APPENDIX B: SUPPORTING INFORMATION

The ellipsometry fit in the UV-visible regime determines an angle of the transition dipole moment of  $17^\circ$  with respect to the surface of the substrate. Two monomers with the oxygen atoms on the same side of the backbone have an angle of about  $7.6^\circ$  to each other, which results in a bending of the backbone. Therefore, it is likely that the polymer exhibits curves with the overall direction parallel to the substrate. This would explain a mean transition dipole moment with a certain angle with respect to the substrate.

Figure 7(a) shows a the same peak on the meridian as in Fig. 3, but with an additional circle, which is attributed to the  $\text{SiO}_2$  shown in Fig. 7(b).

Hence, independently of the used substrate the polymer BBL self-assembles over the whole film thicknesses. Atomic force microscopy (AFM) pictures from both substrates, shown in Figs. 8(a) and 8(b), show also a similar surface topology. Despite the different film thicknesses, both films show grains in the range of 50 nm. Furthermore the film is not closed and shows a large roughness.

The DFT calculations have been performed with the software TURBOMOLE [33–43]. Based on the findings from

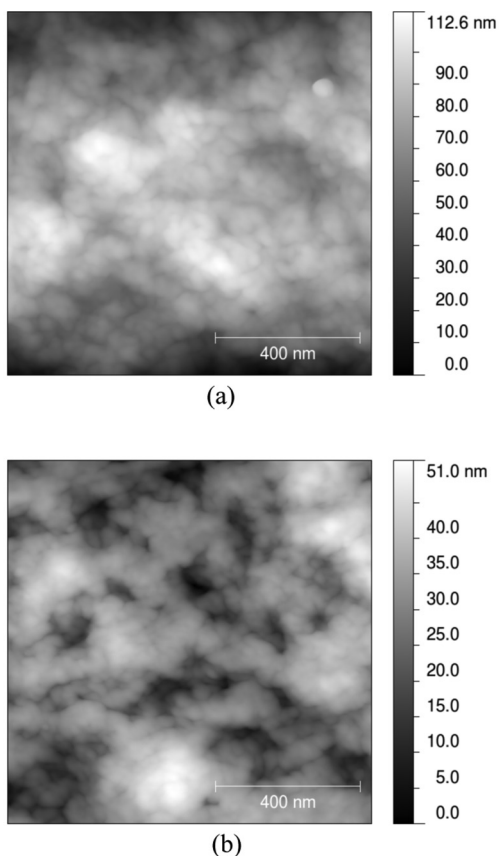


FIG. 8. AFM images of spin-coated BBL on a silicon substrate with native oxide (a) and on a silicon substrate with 1 μm SiO<sub>2</sub> (b), for ellipsometry purposes.

Ruuska [28], Rappoport [53], and the integration of PBE0 in TURBOMOLE, the hybrid functional PBE0 is used.

As shown in Fig. 9, different basis sets show different results. The recommended basis set 6-311++G\*\* and TZVPPD are similar to def2-SVPD. By adding a diffusive part in the basis set the polarizability seems to saturate, which was also reported by Rappoport [53]. Therefore, in order to keep the computational time low, the subsequent calculations will be made with the basis set def2-SVPD.

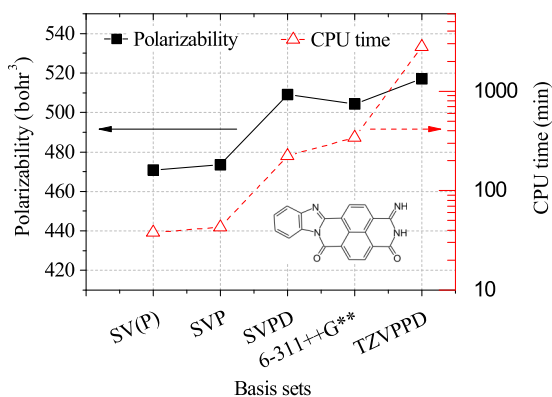


FIG. 9. (Color online) Left: Electronic polarization of a BBL monomer in the *x* direction with the functional PBE0 and different basis sets. Inset: Simulated molecule which reflects one monomer of the polymer BBL.

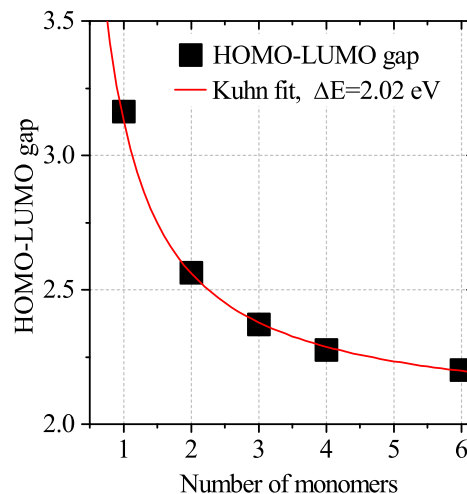


FIG. 10. (Color online) Calculated HOMO-LUMO gaps for different numbers of monomers. For the calculations, def2-SVPD is used as a basis set and PBE0 as the functional. The fit is performed after Kuhn's equation; see main text [54,55].

Figure 10 shows the calculated HOMO-LUMO gap as a function of the polymer length. Kuhn's equation provides a correlation between the molecule length and the HOMO-LUMO gap [54,55]:  $\Delta E = h(N + 1)/[8md(N + L)] + V_0(1 - 1/N)$ , where *h* is Planck's constant, *n* the number of π electrons, *m* the electron mass, *V*<sub>0</sub> the HOMO-LUMO gap (which is identical to Δ*E* for infinite polymers), *L* a parameter to be adjusted, and in a one-dimensional polymer *d* represents the averaged C-C bond length. Using this equation with *d*, *L*, and *V*<sub>0</sub> as fitting parameters, one obtains 2.02 eV for the HOMO-LUMO gap on an infinitely long polymer chain with *d* = 1.17 × 10<sup>-10</sup> m. The reported HOMO-LUMO gap is 1.9 eV [56]. This result shows that not only the polarizability but also the HOMO-LUMO gap needs several monomers to approximate the measured data. The deviation of 0.12 eV could originate from deviations due to DFT approximations. Including the solvent MSA into the DFT simulation by using the COSMO-solvation method of TURBOMOLE, the HOMO-LUMO gap changes by 0.02 eV and therefore has a minor effect.

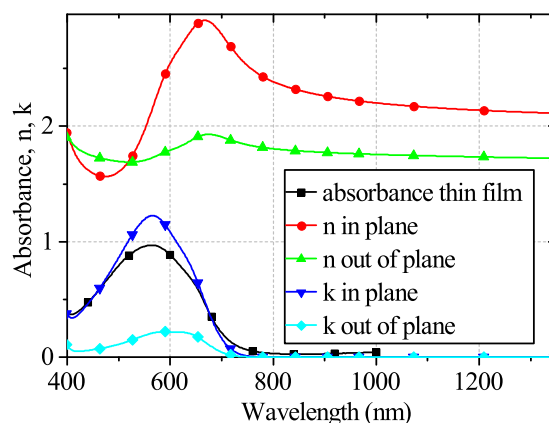


FIG. 11. (Color online) Absorbance of spin-coated BBL and the *n* and *k* values from ellipsometry are shown for comparison.

In Fig. 11 the thin-film absorbance, measured with a two-beam spectrometer UV 3100, Shimadzu Corporation, and the  $n$  and  $k$  values from the UV-visible ellipsometry measurements

are shown for comparison. The similar shape of the in-plane  $k$  value compared to the absorbance spectra supports the validity of the ellipsometric model used.

- 
- [1] J. You, L. Dou, K. Yoshimura, T. Kato, K. Ohya, T. Moriarty, K. Emery, C.-C. Chen, J. Gao, G. Li *et al.*, *Nat. Commun.* **4**, 1446 (2013).
- [2] K. Cnops, B. P. Rand, D. Cheyons, B. Verreet, M. A. Empl, and P. Heremans, *Nat. Commun.* **5**, 3406 (2014).
- [3] O. L. Griffith and S. R. Forrest, *Nano Lett.* **14**, 2353 (2014).
- [4] S. Y. Leblebici, T. L. Chen, P. Olalde-Velasco, W. Yang, and B. Ma, *ACS Appl. Mater. Interfaces* **5**, 10105 (2013).
- [5] N. Cho, C. W. Schlenker, K. M. Kneesting, P. Koelsch, H.-L. Yip, D. S. Ginger, and A. K.-Y. Jen, *Adv. Energy Mater.* **4**, 1301857 (2014).
- [6] N. Camaioni and R. Po, *J. Phys. Chem. Lett.* **4**, 1821 (2013).
- [7] M. Guo, T. Hayakawa, M.-A. Kakimoto, and T. Goodson, *J. Phys. Chem. B* **115**, 13419 (2011).
- [8] S. Adachi, *Optical Properties of Crystalline and Amorphous Semiconductors: Materials and Fundamental Principles* (Springer Science+Business Media, LLC, 1999).
- [9] H. Sobotta, H. Neumann, R. Franzheld, and W. Seifert, *Physica Status Solidi B* **174**, K57 (1992).
- [10] M. Knupfer, J. Fink, E. Zojer, G. Leising, and D. Fichou, *Chem. Phys. Lett.* **318**, 585 (2000).
- [11] J.-W. van der Horst, P. A. Bobbert, M. A. J. Michels, and H. Bässler, *J. Chem. Phys.* **114**, 6950 (2001).
- [12] K. Hummer and C. Ambrosch-Draxl, *Phys. Rev. B* **71**, 081202 (2005).
- [13] M. Knupfer, *Appl. Phys. A: Mater. Sci. Process.* **77**, 623 (2003).
- [14] D. Moses, J. Wang, A. J. Heeger, N. Kirova, and S. Brazovskii, *Proc. Natl. Acad. Sci. USA* **98**, 13496 (2001).
- [15] M. Yoon, A. Facchetti, and T. Marks, *Proc. Natl. Acad. Sci. U.S.A.* **102**, 4678 (2005).
- [16] Y.-Z. Tang, X.-F. Huang, Y.-M. Song, P. W. Hong Chan, and R.-G. Xiong, *Inorg. Chem.* **45**, 4868 (2006).
- [17] W. Demtroder, *Experimentalphysik 3* (Springer, Berlin, 2000).
- [18] H. Sirringhaus, P. J. Brown, R. H. Friend, M. M. Nielsen, K. Bechgaard, B. M. W. Langeveld-Voss, A. J. H. Spiering, R. A. J. Janssen, E. W. Meijer, P. Herwig *et al.*, *Nature (London)* **401**, 685 (1999).
- [19] A. Babel and S. A. Jenekhe, *J. Am. Chem. Soc.* **125**, 13656 (2003).
- [20] F. Arnold and R. V. Deussen, *Macromolecules* **2**, 497 (1969).
- [21] H. Song, A. Fratini, M. Chabiny, G. Price, A. K. Agrawal, C.-S. Wang, J. Burkette, D. S. Dudis, and F. E. Arnold, *Synth. Met.* **69**, 533 (1995).
- [22] A. L. Briseno, S. C. B. Mannsfeld, P. J. Shamberger, F. S. Ohuchi, Z. Bao, S. A. Jenekhe, and Y. Xia, *Chem. Mater.* **20**, 4712 (2008).
- [23] M. Campoy-Quiles, P. G. Etchegoin, and D. D. C. Bradley, *Phys. Rev. B* **72**, 045209 (2005).
- [24] D. Wynands, M. Erber, R. Rentenberger, M. Levichkova, K. Walzer, K.-J. Eichhorn, and M. Stamm, *Org. Electron.* **13**, 885 (2012).
- [25] D. Yokoyama, A. Sakaguchi, M. Suzuki, and C. Adachi, *Appl. Phys. Lett.* **93**, 173302 (2008).
- [26] P. Palfy-Muhoray and D. Balzarini, *Can. J. Phys.* **59**, 375 (1981).
- [27] K. Urano and M. Inoue, *J. Chem. Phys.* **66**, 791 (1977).
- [28] H. Ruuska, E. Arola, K. Kannus, T. T. Rantala, and S. Valkealahti, *J. Chem. Phys.* **128**, 064109 (2008).
- [29] M. Srinivasan and P. Narayanan, *Pramana* **19**, 117 (1982).
- [30] J. Osborn, *Phys. Rev.* **67**, 351 (1945).
- [31] R. H. Boyd and L. Kesner, *Macromolecules* **20**, 1802 (1987).
- [32] A. C. Lasaga and R. T. Cygan, *Am. Mineral.* **67**, 328 (1982).
- [33] K. Eichkorn, F. Weigend, O. Treutler, and R. Ahlrichs, *Theor. Chem. Acc.* **97**, 119 (1997).
- [34] K. Eichkorn, O. Treutler, H. Öhm, M. Häser, and R. Ahlrichs, *Chem. Phys. Lett.* **240**, 283 (1995).
- [35] H. Weiss, R. Ahlrichs, and M. Häser, *J. Chem. Phys.* **99**, 1262 (1993).
- [36] C. Ochsenfeld, J. Gauss, and R. Ahlrichs, *J. Chem. Phys.* **103**, 7401 (1995).
- [37] R. Bauernschmitt and R. Ahlrichs, *J. Chem. Phys.* **104**, 9047 (1996).
- [38] R. Bauernschmitt, M. Häser, O. Treutler, and R. Ahlrichs, *Chem. Phys. Lett.* **264**, 573 (1997).
- [39] F. Furche and D. Rappoport, *Theoretical and Computational Chemistry* **16**, 93 (2005).
- [40] O. Treutler and R. Ahlrichs, *J. Chem. Phys.* **102**, 346 (1995).
- [41] M. Von Arnim and R. Ahlrichs, *J. Comput. Chem.* **19**, 1746 (1998).
- [42] J. E. Bates and F. Furche, *J. Chem. Phys.* **137**, 164105 (2012).
- [43] M. Kühn and F. Weigend, *ChemPhysChem* **12**, 3331 (2011).
- [44] B. Kirtman, *Chem. Phys. Lett.* **143**, 81 (1988).
- [45] S. Nir, S. Adams, and R. Rein, *J. Chem. Phys.* **59**, 3341 (1973).
- [46] B. Champagne, D. H. Mosley, and J.-M. André, *Int. J. Quantum Chem.* **48**, 667 (1993).
- [47] R. Azzam and N. M. Bashara, *Ellipsometry and Polarized Light* (Elsevier Science Publishing Co., Inc., Amsterdam, 1987).
- [48] H. Fujiwara, *Spectroscopic Ellipsometry: Principles and Applications* (John Wiley & Sons, Inc., Chichester, UK, 2007).
- [49] K. Hinrichs and K. J. Eichhorn, *Ellipsometry of Functional Organic Surfaces and Films* (Springer, Heidelberg, 2014).
- [50] A. Röseler and E. H. Korte, in *Handbook of Vibrational Spectroscopy*, edited by P. R. Griffiths and J. Chalmers (Wiley, Chichester, 2001), Chap. 2.8.
- [51] K. Hinrichs, M. Gensch, and N. Esser, *Appl. Spectrosc.* **59**, 272A (2005).
- [52] K. Hinrichs, M. Levichkova, D. Wynands, K. Walzer, K. J. Eichhorn, P. Bäuerle, K. Leo, and M. Riede, *Thin Solid Films* **525**, 97 (2012).
- [53] D. Rappoport and F. Furche, *J. Chem. Phys.* **133**, 134105 (2010).
- [54] J. S. de Melo, L. M. Silva, L. G. Arnaut, and R. S. Becker, *J. Chem. Phys.* **111**, 5427 (1999).
- [55] H. Kuhn, *J. Chem. Phys.* **17**, 1198 (1949).
- [56] S. A. Jenekhe and S. Yi, *Appl. Phys. Lett.* **77**, 2635 (2000).